Journal of Solid Mechanics Vol. 4, No. 2 (2012) pp. 177-194

Nonlinear Finite Element Eccentric Low-Velocity Impact Analysis of Rectangular Laminated Composite Plates Subjected to In-phase/Anti-phase Biaxial Preloads

M. Shariyat*, M. Moradi, S. Samaee

Faculty of Mechanical Engineering, K.N. Toosi University of Technology, Tehran 19991-43344, Iran

Received 8 April 2012; accepted 5 June 2012

ABSTRACT

All impact analyses performed so far for the composite plates, have treated central impacts. Furthermore, investigations on influences of the in-plane biaxial compression, tension, or tension-compression preloads on various responses of the low-velocity impact, especially the indentation, have not been performed so far. In the present research, a finite element formulation is presented for response prediction of a low-velocity eccentric impact between a rigid spherical indenter and a laminated composite rectangular plate with asymmetric lamination scheme. Different contact laws are considered for the loading and unloading phases. A parametric study is performed to investigate influence of the specifications of the plates and the indenter, the eccentric value, and the in-plane preloads on the indentation and force time histories. Results show that the compressive and tensile in-plane preloads reduce and increase the contact force (and consequently, the indentation values), respectively. Therefore, the extensive tensile preloads may lead to higher damages.

Keywords: Finite element; Eccentric low-velocity impact; Composite plate; Contact law; Preload

1 INTRODUCTION

MANY load carrying composite structures, often in the form of thin-walled components, are vulnerable to impacts with rigid indenters. The composite plates used in construction of the external or internal portions of the structures of the ground, space, aerospace, and marine vehicles may experience low-velocity impacts with rigid foreign indenters during their service lives. Although many papers have been published on investigation of various aspects of the low-velocity impact of the composite plates, there are still some important aspects, such as impact eccentricity and preloads that have not been fully investigated.

Some researchers have employed discrete models for behavior simulation of plates subjected to low-velocity impacts. However, these models cannot incorporate effects of the higher vibration modes whose effects are in some cases comparable to those of the fundamental vibration mode of the plate. Gong and Lam [1] used a discrete model with two degrees-of-freedom in order to determine the history of the contact force. Jacquelin et al. [2] presented an extended single degree-of-freedom model for the impacted structures. Pashah et al. [3] provided guidelines for prediction of the structural responses on the basis of the impact time duration and the fundamental period of the impacted structure through using discrete models. Anderson [4] used a single-degree-of-freedom model for analyzing large mass impacts on composite sandwich laminates. Abrate [5,6] has comprehensively reviewed various

* Corresponding author. Tel.: +98 9122727199; Fax: +98 21 88674748.
E-mail address: shariyat@kntu.ac.ir and m_shariyat@yahoo.com (M.Shariyat).

models of impact of the sandwich and composite structures. Chai and Zhu [7] reviewed the research progress on dynamic response of composite sandwich structures subjected to low-velocity impacts. Qiu and Yu [8] reviewed some topics related to the advances and applications of the structural impact dynamics in recent years.

Some of the researches performed on the basis of the consistent continuous models, have investigated the global displacements and/or forces. Therefore, local deformations of the contact region and the relevant local effects are have been ignored. Therefore, only the global displacements or stresses of the structure have been of concern [9,10]. Some others have analyzed plates without lateral movability (e.g., plates resting on rigid substrates). They mainly assumed that deformations of the impacted region of the plate conform to the indenter surface [11-15].

Apart from the geometrically consistent models, models based on Hertzian-type contact laws have also been developed. Guan and Yang [16] and Zheng and Binienda [17] used modified Hertzian contact laws. For orthotropic plates, it has been assumed that the contact pressure and contact area could be obtained from the usual formulas for isotropic materials, but with the isotropic modulus of elasticity replaced by the orthotropic modulus in the loading direction. Olsson [18] presented an analytical model for small mass impact on orthotropic laminated composite plates.

Very rare researches have investigated influence of the initial stresses on the dynamic [19] or low-velocity impact responses of the rectangular [20,21] or circular [22] plates. Khalili et al. [23] discussed transverse impact response of a composite plate with an in-plane biaxial tension. Sveklo-Hertz contact law for the orthotropic materials was used to describe the interaction between the plate and the indenter. Heimbs et al. [24] reported experimental and LS-DYNA finite element results for the rectangular plates. Choi [25] studied low-velocity eccentric impact of composite plates subjected to in-plane preloads. However, the reported results do not enable a clear conclusion, because the results were oscillatory and almost no effects have been observed on the indentation value.

The foregoing brief review reveals that the previous researches focused on centric low-velocity impacts. Furthermore, influences of the compression, extension, or extension-compression in-plane biaxial preloads on various responses of the low-velocity impact, especially the indentation, have not been fully investigated so far. In the present research, a finite element formulation is presented for response prediction of a low-velocity eccentric impact between a rigid spherical indenter and a laminated composite rectangular plate with asymmetric lamination scheme. Different contact laws are considered for the loading and unloading phases. A parametric study is performed to investigate influence of the specifications of the plate and the indenter, the eccentric value, and the in-plane preloads on the indentation and contact force time histories.

2 THE GOVERNING EQUATIONS

2.1 The apparent modulus of elasticity of the contact region based on the global-local approach

Consider a rectangular plate whose geometric parameters and coordinate system are shown in Fig. 1. In-plane dimensions and thickness of the plate are denoted by a, b, and h, respectively. The plate is impacted by a spherical indenter or a projectile with a spherical nose whose initial velocity and radius are denoted by v_0 and R, respectively.

The stress-strain relation of the kth layer of the plate in the material coordinate may be written as [26]:

$$\begin{Bmatrix}\sigma_1\\ \sigma_2\\ \sigma_4\\ \sigma_5\\ \sigma_6\end{Bmatrix}^{(k)} = \begin{bmatrix} Q_{11} & Q_{12} & 0 & 0 & 0\\ Q_{12} & Q_{22} & 0 & 0 & 0\\ 0 & 0 & Q_{44} & 0 & 0\\ 0 & 0 & 0 & Q_{55} & 0\\ 0 & 0 & 0 & 0 & Q_{66}\end{bmatrix}^{(k)} \begin{Bmatrix}\varepsilon_1\\ \varepsilon_2\\ \varepsilon_4\\ \varepsilon_5\\ \varepsilon_6\end{Bmatrix}^{(k)} \tag{1}$$

where

$$Q_{11}^{(k)} = \frac{E_1^{(k)}}{1-\nu_{12}^{(k)}\nu_{21}^{(k)}},\quad Q_{12}^{(k)} = \frac{\upsilon_{12}^{(k)}E_2^{(k)}}{1-\nu_{12}^{(k)}\nu_{21}^{(k)}},\quad Q_{22}^{(k)} = \frac{E_2^{(k)}}{1-\nu_{12}^{(k)}\nu_{21}^{(k)}},\quad Q_{44}^{(k)} = G_{23}^{(k)},\quad Q_{55}^{(k)} = G_{13}^{(k)}, Q_{66}^{(k)} = G_{12}^{(k)},\quad \frac{\nu_{12}}{E_1} = \frac{\nu_{21}}{E_2} \tag{2}$$

where the first two stress/strain components are normal components and the remaining components are shear ones.

If the material axis, in-plate transverse direction, and out-of-plane transverse direction are denoted by *X*, *Y*, and *Z*, one has for example:

$$\boldsymbol{\sigma}^T = \langle \sigma_X \quad \sigma_Y \quad \tau_{YZ} \quad \tau_{XZ} \quad \tau_{XY} \rangle \tag{3}$$

If the fiber angle with the geometric *x* axis is denoted by θ, the stress-strain relation in the geometric coordinates may be expressed as [26]:

$$\begin{Bmatrix} \sigma_x \\ \sigma_y \\ \tau_{yz} \\ \tau_{xz} \\ \tau_{xy} \end{Bmatrix}^{(k)} = \begin{bmatrix} \bar{Q}_{11} & \bar{Q}_{12} & 0 & 0 & \bar{Q}_{16} \\ \bar{Q}_{12} & \bar{Q}_{22} & 0 & 0 & \bar{Q}_{26} \\ 0 & 0 & \bar{Q}_{44} & \bar{Q}_{45} & 0 \\ 0 & 0 & \bar{Q}_{45} & \bar{Q}_{55} & 0 \\ \bar{Q}_{16} & \bar{Q}_{26} & 0 & 0 & \bar{Q}_{66} \end{bmatrix}^{(k)} \begin{Bmatrix} \varepsilon_x \\ \varepsilon_y \\ \gamma_{yz} \\ \gamma_{xz} \\ \gamma_{xy} \end{Bmatrix}^{(k)} \tag{4}$$

where

$$\begin{aligned}
\bar{Q}_{11} &= Q_{11}\cos^4\theta + 2\left(Q_{12}+2Q_{66}\right)\sin^2\theta\cos^2\theta + Q_{22}\sin^4\theta \\
\bar{Q}_{12} &= \left(Q_{11}+Q_{22}-4Q_{66}\right)\sin^2\theta\cos^2\theta + Q_{12}\left(\sin^4\theta+\cos^4\theta\right) \\
\bar{Q}_{22} &= Q_{11}\sin^4\theta + 2\left(Q_{12}+2Q_{66}\right)\sin^2\theta\cos^2\theta + Q_{22}\cos^4\theta \\
\bar{Q}_{16} &= \left(Q_{11}-Q_{12}-2Q_{66}\right)\sin\theta\cos^3\theta + \left(Q_{12}-Q_{22}+2Q_{66}\right)\sin^3\theta\cos\theta \\
\bar{Q}_{26} &= \left(Q_{11}-Q_{12}-2Q_{66}\right)\sin^3\theta\cos\theta + \left(Q_{12}-Q_{22}+2Q_{66}\right)\sin\theta\cos^3\theta \\
\bar{Q}_{44} &= Q_{44}\cos^2\theta + Q_{55}\sin^2\theta \\
\bar{Q}_{45} &= \left(Q_{55}-Q_{44}\right)\cos\theta\sin\theta \\
\bar{Q}_{55} &= Q_{55}\cos^2\theta + Q_{44}\sin^2\theta \\
\bar{Q}_{66} &= \left(Q_{11}+Q_{22}-2Q_{12}-2Q_{66}\right)\sin^2\theta\cos^2\theta + Q_{66}\left(\sin^4\theta+\cos^4\theta\right)
\end{aligned} \tag{5}$$

Turner [27] claimed that for a transversely isotropic plate impacted by a rigid spherical indenter, the contact force may be related through the contact stiffness to the indentation value as follows:

$$\begin{aligned}
F &= k_c \alpha^{\frac{3}{2}} \\
k_c &= \frac{4}{3}\sqrt{R}.E_T^*
\end{aligned} \tag{6}$$

where α is the indentation value and E_T^* is the effective modulus:

$$E_T^* = \frac{2}{\lambda_1\lambda_3} \tag{7}$$

where

$$\lambda_1 = \left(\frac{E_x/E_y - \nu_{xz}^2}{1-\nu_{xy}^2}\right)^{1/2}, \quad \lambda_2 = \frac{1+\left(\frac{E_x}{2G_{xz}}-1\right)-\nu_{xz}\left(1+\nu_{xy}\right)}{1-\nu_{xy}^2}, \quad \lambda_3 = \frac{1-\nu_{xy}}{G_{xy}}\left(\frac{\lambda_1+\lambda_2}{2}\right)^{1/2} \tag{8}$$

Therefore

$$\alpha = \left(\frac{3F}{4\sqrt{R}E_T^*}\right)^{2/3}, \quad \left(k_c\right)_{eff} = \frac{4}{3}\sqrt{R}E_T^* \tag{9}$$

For a multilayered composite plate, effect of the underneath layers may be incorporated through using the apparent stiffness concept. It is evident that the stiffness of the lower layers can affect stiffness of the contact region. For this reason, some researchers have proposed using the integral mean of the stiffness of the layers [22].

For the unloading phase, the modified Hertzian contact law proposed by Yang and Sun [28] is employed. In this regard, the indentation force of Eq. (6) has to be substituted by:

$$F = F_{\max}\left(\frac{\alpha-\alpha_0}{\alpha_{\max}-\alpha_0}\right)^{5/2} \tag{10}$$

for the unloading phase, where $F_{\max}$ is the maximum contact force reached during the impact, $\alpha_{\max}$ is the maximum indentation which corresponds to $F_{\max}$ and α_0 is the permanent indentation, if any.

3 THE GOVERNING EQUATIONS OF IMPACT OF THE PRELOADED PLATE

Based on Mindlin's first-order shear deformation theory, the displacement field of the plate may be described as [26]:

$$\begin{cases} u(x,y,t) = u_0(x,y,t) + z\varphi_x(x,y,t) \\ v(x,y,t) = v_0(x,y,t) + z\varphi_y(x,y,t) \\ w(x,y,t) = w_0(x,y,t) \end{cases} \tag{11}$$

where u_0, v_0, and w_0 are displacements of the reference plane of the plate and φ_x and φ_y are rotations of the cross section relative to x and y axes, respectively.

Using von Karman-type assumptions, strain components of the reference plane of the plate may be related to the displacement components of the mentioned plane through the following nonlinear relations:

$$\boldsymbol{\varepsilon} = \begin{Bmatrix} \varepsilon_{xx} \\ \varepsilon_{yy} \\ \gamma_{yz} \\ \gamma_{xz} \\ \gamma_{xx} \end{Bmatrix} = \begin{Bmatrix} \dfrac{\partial u_0}{\partial x} + \dfrac{1}{2}\left(\dfrac{\partial w_0}{\partial x}\right)^2 \\ \dfrac{\partial v_0}{\partial y} + \dfrac{1}{2}\left(\dfrac{\partial w_0}{\partial y}\right)^2 \\ \dfrac{\partial w_0}{\partial x} + \varphi_x \\ \dfrac{\partial w_0}{\partial y} + \varphi_y \\ \dfrac{\partial u_0}{\partial x} + \dfrac{\partial v_0}{\partial y} + \dfrac{\partial w_0}{\partial x}\dfrac{\partial w_0}{\partial y} \end{Bmatrix} + z\begin{Bmatrix} \dfrac{\partial \varphi_x}{\partial x} \\ \dfrac{\partial \varphi_y}{\partial y} \\ 0 \\ 0 \\ \dfrac{\partial \varphi_x}{\partial x} + \dfrac{\partial \varphi_y}{\partial y} \end{Bmatrix} \tag{12}$$

The governing equations may be derived using Hamilton's principle [26]:

$$\int_0^T \left(\delta U + \delta V - \delta TK\right) dt = 0 \tag{13}$$

Increments of the strain energy δU, work of the external loads δV, and the kinematic energy δK may be determined from:

$$\begin{aligned} \delta U &= \int_{\Omega_0}\int_{-h/2}^{h/2} \boldsymbol{\delta\varepsilon}^T \boldsymbol{\sigma}.dz\, d\Omega_0 = \int_{\Omega_0}\left\{\int_{-h/2}^{h/2}\left[\sigma_{xx}\delta\varepsilon_{xx} + \sigma_{yy}\delta\varepsilon_{yy} + \sigma_{xy}\delta\gamma_{xy} + \sigma_{xz}\delta\gamma_{xz} + \sigma_{yz}\delta\gamma_{yz}\right]dz\right\}dxdy \\ &= \int_{\Omega_0}\left(\boldsymbol{\delta\varepsilon}^{0T}\int_{-h/2}^{h/2}\boldsymbol{\sigma}.dz + \boldsymbol{\delta\varepsilon}^{1T}\int_{-h/2}^{h/2}\boldsymbol{\sigma}.z.dz\right)d\Omega_0 \end{aligned} \tag{14}$$

$$\delta V = -\int_{\Omega_0} q w_0 dxdy - \int_{\Gamma_\sigma}\int_{-h/2}^{h/2}\left[\hat{\sigma}_{nn}\left(\delta u_n + z\delta\phi_n\right) + \hat{\sigma}_{ns}\left(\delta u_s + z\delta\phi_s\right) + \hat{\sigma}_{nz}\delta w_0\right] dz\, ds - F_c \delta w_{0,i} \tag{15}$$

$$\delta K = \int_{\Omega_0}\int_{-h/2}^{h/2}\rho_0\left[\left(\dot{u}_0 + z\dot{\varphi}_x\right)\left(\delta\dot{u}_0 + z\delta\dot{\varphi}_x\right) + \left(\dot{v}_0 + z\dot{\varphi}_y\right)\left(\delta\dot{v}_0 + z\delta\dot{\varphi}_y\right) + \dot{w}_0\delta\dot{w}_0\right] dz.dx\, dy \tag{16}$$

where Ω_0 and Γ_σ represent the reference plane area and the plate boundary and the subscripts, *n* and, *s* ,and *i* denote directions normal and tangent to the boundary, and the indenter respectively. Substituting Eqs. (14-16) into Eq. (13), using the following definitions:

$$\begin{Bmatrix} N_{xx} \\ N_{yy} \\ N_{xy} \end{Bmatrix} = \int_{-\frac{h}{2}}^{\frac{h}{2}} \begin{Bmatrix} \sigma_{xx} \\ \sigma_{yy} \\ \sigma_{xy} \end{Bmatrix} dz, \qquad \begin{Bmatrix} M_{xx} \\ M_{yy} \\ M_{xy} \end{Bmatrix} = \int_{-\frac{h}{2}}^{\frac{h}{2}} \begin{Bmatrix} \sigma_{xx} \\ \sigma_{yy} \\ \sigma_{xy} \end{Bmatrix} z\, dz$$

$$\begin{Bmatrix} \hat{N}_{nn} \\ \hat{N}_{ns} \end{Bmatrix} = \int_{-\frac{h}{2}}^{\frac{h}{2}} \begin{Bmatrix} \hat{\sigma}_{nn} \\ \hat{\sigma}_{ns} \end{Bmatrix} dz, \qquad \begin{Bmatrix} \hat{M}_{nn} \\ \hat{M}_{ns} \end{Bmatrix} = \int_{-\frac{h}{2}}^{\frac{h}{2}} \begin{Bmatrix} \hat{\sigma}_{nn} \\ \hat{\sigma}_{ns} \end{Bmatrix} z dz \tag{17}$$

$$\begin{Bmatrix} I_0 \\ I_1 \\ I_2 \end{Bmatrix} = \int_{-\frac{h}{2}}^{\frac{h}{2}} \begin{Bmatrix} 1 \\ z \\ z^2 \end{Bmatrix} \rho_0\, dz, \qquad \hat{Q}_n = \int_{-\frac{h}{2}}^{\frac{h}{2}} \hat{\sigma}_{nz} dz$$

Leads to

$$\begin{aligned} \int_0^T \Bigg\{ \int_{\Omega_0} \Bigg[& N_{xx}\left(\frac{\partial\delta u_0}{\partial x} + \frac{\partial w_0}{\partial x}\frac{\partial\delta w_0}{\partial x}\right) + M_{xx}\frac{\partial\delta\varphi_x}{\partial x} + N_{yy}\left(\frac{\partial\delta v_0}{\partial y} + \frac{\partial w_0}{\partial y}\frac{\partial\delta w_0}{\partial y}\right) + M_{yy}\frac{\partial\delta\varphi_y}{\partial y} \\ & + N_{xy}\left(\frac{\partial\delta u_0}{\partial y} + \frac{\partial\delta v_0}{\partial x} + \frac{\partial w_0}{\partial y}\frac{\partial\delta w_0}{\partial x} + \frac{\partial w_0}{\partial x}\frac{\partial\delta w_0}{\partial y}\right) + M_{xy}\left(\frac{\partial\delta\varphi_x}{\partial y} + \frac{\partial\delta\varphi_y}{\partial x}\right) \\ & + Q_x\left(\frac{\partial\delta w_0}{\partial x} + \delta\varphi_x\right) + Q_y\left(\frac{\partial\delta w_0}{\partial y} + \delta\varphi_y\right) - q\delta w_0 - F_c\delta w_{0,i} - I_0\left(\dot{u}_0\delta\dot{u}_0 + \dot{v}_0\delta\dot{v}_0 + \dot{w}_0\delta\dot{w}_0\right) \\ & - I_1\left(\dot{\varphi}_x\delta\dot{u}_0 + \dot{\varphi}_y\delta\dot{v}_0 + \delta\dot{\varphi}_x\dot{u}_0 + \delta\dot{\varphi}_y\dot{v}_0\right) - I_2\left(\dot{\varphi}_x\delta\dot{\varphi}_x + \dot{\varphi}_y\delta\dot{\varphi}_y\right)\Bigg] dxdy \\ & - \int_{\Gamma_\sigma}\left(\hat{N}_{nn}\delta u_n + \hat{N}_{ns}\delta u_s + \hat{M}_{nn}\delta\phi_n + \hat{M}_{ns}\delta\phi_s + \hat{Q}_n\delta w_0\right) dS \Bigg\} dt = 0 \end{aligned} \tag{18}$$

On the other hand:

$$\begin{aligned} & -\int_0^T\int_{\Omega_0} I_0\left(\dot{u}_0\delta\dot{u}_0 + \dot{v}_0\delta\dot{v}_0 + \dot{w}_0\delta\dot{w}_0\right) dxdydt \\ & = \int_0^T\int_{\Omega_0} I_0\left(\ddot{u}_0\delta u_0 + \ddot{v}_0\delta v_0 + \ddot{w}_0\delta w_0\right) dxdydt - \left(\int_{\Omega_0} I_0\left(\dot{u}_0\delta u_0 + \dot{v}_0\delta v_0 + \dot{w}_0\delta w_0\right) dxdy\right)_0^T \\ & = \int_0^T\int_{\Omega_0} I_0\left(\ddot{u}_0\delta u_0 + \ddot{v}_0\delta v_0 + \ddot{w}_0\delta w_0\right) dxdydt \end{aligned} \tag{19}$$

Because $\delta\boldsymbol{D}_0(\boldsymbol{X},T) = \delta\boldsymbol{D}_0(\boldsymbol{X},0) = 0$, where $\boldsymbol{D}_0$ is the displacement vector. The results may be confirmed noting that the result of Eq. (19) is (negative of) the work of the translational inertia forces. In a similar manner:

$$-\int_0^T\int_{\Omega_0} -I_1\left(\dot{\varphi}_x\delta\dot{u}_0+\dot{\varphi}_y\delta\dot{v}_0+\delta\dot{\varphi}_x\dot{u}_0+\delta\dot{\varphi}_y\dot{v}_0\right)dxdydt=\int_0^T\int_{\Omega_0} I_0\left(\ddot{\varphi}_x\delta u_0+\ddot{\varphi}_y\delta v_0+\delta\varphi_x\ddot{u}_0+\delta\varphi_y\ddot{v}_0\right)dxdydt \tag{20}$$

and

$$-\int_0^T\int_{\Omega_0} I_2\left(\dot{\varphi}_x\delta\dot{\varphi}_x+\dot{\varphi}_y\delta\dot{\varphi}_y\right)dxdydt=\int_0^T\int_{\Omega_0} I_2\left(\ddot{\varphi}_x\delta\varphi_x+\ddot{\varphi}_y\delta\varphi_y\right)dxdydt \tag{21}$$

Hence, Eq. (18) may be rewritten as:

$$\begin{aligned}\int_0^T\Bigg\{\int_{\Omega_0}\Bigg[&N_{xx}\left(\frac{\partial\delta u_0}{\partial x}+\frac{\partial w_0}{\partial x}\frac{\partial\delta w_0}{\partial x}\right)+N_{yy}\left(\frac{\partial\delta v_0}{\partial y}+\frac{\partial w_0}{\partial y}\frac{\partial\delta w_0}{\partial y}\right)\\&+N_{xy}\left(\frac{\partial\delta u_0}{\partial y}+\frac{\partial\delta v_0}{\partial x}+\frac{\partial w_0}{\partial y}\frac{\partial\delta w_0}{\partial x}+\frac{\partial w_0}{\partial x}\frac{\partial\delta w_0}{\partial y}\right)+M_{xx}\frac{\partial\delta\varphi_x}{\partial x}+M_{yy}\frac{\partial\delta\varphi_y}{\partial y}\\&+M_{xy}\left(\frac{\partial\delta\varphi_x}{\partial y}+\frac{\partial\delta\varphi_y}{\partial x}\right)+Q_x\left(\frac{\partial\delta w_0}{\partial x}+\delta\varphi_x\right)+Q_y\left(\frac{\partial\delta w_0}{\partial y}+\delta\varphi_y\right)-q\delta w_0-F_c\delta w_{0,i}\\&+I_0\left(\ddot{u}_0\delta u_0+\ddot{v}_0\delta v_0+\ddot{w}_0\delta w_0\right)+I_1\left(\ddot{\varphi}_x\delta u_0+\ddot{\varphi}_y\delta v_0+\delta\varphi_x\ddot{u}_0+\delta\varphi_y\ddot{v}_0\right)\\&+I_2\left(\ddot{\varphi}_x\delta\varphi_x+\ddot{\varphi}_y\delta\varphi_y\right)\Bigg]dxdy-\int_{\Gamma_\sigma}\left(\hat{N}_{nn}\delta u_n+\hat{N}_{ns}\delta u_s+\hat{M}_{nn}\delta\varphi_n+\hat{M}_{ns}\delta\varphi_s+\hat{Q}_n\delta w_0\right)dS\Bigg\}dt=0\end{aligned} \tag{22}$$

Substituting Eq. (12) into Eq. (17) leads to:

$$\begin{aligned}\begin{Bmatrix}N_{xx}\\N_{yy}\\N_{xy}\end{Bmatrix}&=\begin{bmatrix}A_{11}&A_{12}&A_{16}\\A_{21}&A_{22}&A_{26}\\A_{61}&A_{62}&A_{66}\end{bmatrix}\begin{Bmatrix}\frac{\partial u_0}{\partial x}+\frac{1}{2}\left(\frac{\partial w_0}{\partial x}\right)^2\\\frac{\partial v_0}{\partial y}+\frac{1}{2}\left(\frac{\partial w_0}{\partial y}\right)^2\\\frac{\partial u_0}{\partial x}+\frac{\partial v_0}{\partial y}+\frac{\partial w_0}{\partial x}\frac{\partial w_0}{\partial y}\end{Bmatrix}+\begin{bmatrix}B_{11}&B_{12}&B_{16}\\B_{21}&B_{22}&B_{26}\\B_{61}&B_{62}&B_{66}\end{bmatrix}\begin{Bmatrix}\frac{\partial\varphi_x}{\partial x}\\\frac{\partial\varphi_y}{\partial y}\\\frac{\partial\varphi_x}{\partial x}+\frac{\partial\varphi_y}{\partial y}\end{Bmatrix}\\\begin{Bmatrix}M_{xx}\\M_{yy}\\M_{xyy}\end{Bmatrix}&=\begin{bmatrix}B_{11}&B_{12}&B_{16}\\B_{21}&B_{22}&B_{26}\\B_{61}&B_{62}&B_{66}\end{bmatrix}\begin{Bmatrix}\frac{\partial u_0}{\partial x}+\frac{1}{2}\left(\frac{\partial w_0}{\partial x}\right)^2\\\frac{\partial v_0}{\partial y}+\frac{1}{2}\left(\frac{\partial w_0}{\partial y}\right)^2\\\frac{\partial u_0}{\partial x}+\frac{\partial v_0}{\partial y}+\frac{\partial w_0}{\partial x}\frac{\partial w_0}{\partial y}\end{Bmatrix}+\begin{bmatrix}D_{11}&D_{12}&D_{16}\\D_{21}&D_{22}&D_{26}\\D_{61}&D_{62}&D_{66}\end{bmatrix}\begin{Bmatrix}\frac{\partial\varphi_x}{\partial x}\\\frac{\partial\varphi_y}{\partial y}\\\frac{\partial\varphi_x}{\partial x}+\frac{\partial\varphi_y}{\partial y}\end{Bmatrix}\\\begin{Bmatrix}Q_x\\Q_y\end{Bmatrix}&=k\begin{bmatrix}A_{55}&A_{45}\\A_{45}&A_{44}\end{bmatrix}=k\boldsymbol{A}^*\begin{Bmatrix}\frac{\partial w_0}{\partial x}+\varphi_x\\\frac{\partial w_0}{\partial y}+\varphi_y\end{Bmatrix}\end{aligned} \tag{23}$$

where $k=5/6$ is the shear correction factor [26] and. The following quantities are defined to present compact forms for the next equations:

$$\boldsymbol{A}^{*}=\begin{bmatrix} A_{55} & A_{45} \\ A_{45} & A_{44} \end{bmatrix}, \quad \begin{cases} \varphi_n=\varphi_x n_x+\varphi_y n_y, \;\; \varphi_s=\varphi_y n_x-\varphi_x n_y \\ u_n=u_0 n_x+v_0 n_y, \;\; u_s=v_0 n_x-u_0 n_y \end{cases}$$

$$\boldsymbol{L}_1=\begin{bmatrix} \frac{\partial}{\partial x} & 0 & \frac{\partial w_0}{\partial x}\frac{\partial}{\partial x} & 0 & 0 \\ 0 & \frac{\partial}{\partial y} & \frac{\partial w_0}{\partial y}\frac{\partial}{\partial y} & 0 & 0 \\ \frac{\partial}{\partial y} & \frac{\partial}{\partial x} & \left(\frac{\partial w_0}{\partial x}\right)\frac{\partial}{\partial x}+\left(\frac{\partial w_0}{\partial y}\right)\frac{\partial}{\partial y} & 0 & 0 \end{bmatrix}, \quad \boldsymbol{L}_2=\begin{bmatrix} \frac{\partial}{\partial x} & 0 & \frac{1}{2}\frac{\partial w_0}{\partial x}\frac{\partial}{\partial x} & 0 & 0 \\ 0 & \frac{\partial}{\partial y} & \frac{1}{2}\frac{\partial w_0}{\partial y}\frac{\partial}{\partial y} & 0 & 0 \\ \frac{\partial}{\partial y} & \frac{\partial}{\partial x} & \left(\frac{\partial w_0}{\partial y}\right)\frac{\partial}{\partial y} & 0 & 0 \end{bmatrix},$$

$$\boldsymbol{L}_3=\begin{bmatrix} 0 & 0 & 0 & \frac{\partial}{\partial x} & 0 \\ 0 & 0 & 0 & 0 & \frac{\partial}{\partial y} \\ 0 & 0 & 0 & \frac{\partial}{\partial y} & \frac{\partial}{\partial x} \end{bmatrix}, \quad \boldsymbol{L}_4=\begin{bmatrix} 0 & 0 & \frac{\partial}{\partial x} & 1 & 0 \\ 0 & 0 & \frac{\partial}{\partial y} & 0 & 1 \end{bmatrix}, \quad \boldsymbol{I}=\begin{bmatrix} I_0 & 0 & 0 & I_1 & 0 \\ 0 & I_0 & 0 & 0 & I_1 \\ 0 & 0 & I_0 & 0 & 0 \\ I_1 & 0 & 0 & I_2 & 0 \\ 0 & I_1 & 0 & 0 & I_2 \end{bmatrix} \tag{24}$$

$$\boldsymbol{D}_0=\begin{Bmatrix} u_0 \\ v_0 \\ w_0 \\ \varphi_x \\ \varphi_y \end{Bmatrix}, \quad \boldsymbol{q}=\begin{Bmatrix} 0 \\ 0 \\ q \\ 0 \\ 0 \end{Bmatrix}, \quad \boldsymbol{F}_c=\begin{Bmatrix} 0 \\ 0 \\ F_c \\ 0 \\ 0 \end{Bmatrix}$$

Therefore

$$\boldsymbol{N}=\begin{Bmatrix} N_{xx} \\ N_{yy} \\ N_{xy} \end{Bmatrix}=\left(\boldsymbol{A}\boldsymbol{L}_2+\boldsymbol{B}\boldsymbol{L}_3\right)\boldsymbol{D}_0, \quad \boldsymbol{M}=\begin{Bmatrix} M_{xx} \\ M_{yy} \\ M_{xy} \end{Bmatrix}=\left(\boldsymbol{B}\boldsymbol{L}_2+\boldsymbol{D}\boldsymbol{L}_3\right)\boldsymbol{D}_0, \quad \boldsymbol{Q}=\begin{Bmatrix} Q_x \\ Q_y \end{Bmatrix}=k\boldsymbol{A}^{*}\left(\boldsymbol{L}_4\boldsymbol{D}_0\right) \tag{25}$$

Based on Eq. (25), Eq. (22) may be rewritten as:

$$\int_0^T\Bigg\{\int_{\Omega_0}\Big[\left(\boldsymbol{L}_1\delta\boldsymbol{D}_0\right)^T\left(\boldsymbol{A}\boldsymbol{L}_2+\boldsymbol{B}\boldsymbol{L}_3\right)\boldsymbol{D}_0+\left(\boldsymbol{L}_3\delta\boldsymbol{D}_0\right)^T\left(\boldsymbol{B}\boldsymbol{L}_2+\boldsymbol{D}\boldsymbol{L}_3\right)\boldsymbol{D}_0+\left(\boldsymbol{L}_4\delta\boldsymbol{D}_0\right)^T k\boldsymbol{A}^{*}\left(\boldsymbol{L}_4\boldsymbol{D}_0\right)$$
$$+\left(\delta\boldsymbol{D}_0\right)^T\boldsymbol{I}\left(\ddot{\boldsymbol{D}}_0\right)-\left(\delta\boldsymbol{D}_0\right)^T\boldsymbol{q}\Big]d\Omega_0-\int_{\Gamma_\sigma}\left[\left(\delta\boldsymbol{D}_0\right)^T\boldsymbol{R}^T\boldsymbol{F}_{\boldsymbol{B}}\right]dS-\left(\delta\boldsymbol{D}_0\right)^T\boldsymbol{F}_c\Bigg\}\,\mathrm{dt}=0 \tag{26}$$

On the other hand, based on Eqs. (24,25) one may write:

$$\boldsymbol{D}_{\boldsymbol{n}}=\begin{Bmatrix} u_n \\ u_s \\ w_0 \\ \varphi_n \\ \varphi_s \end{Bmatrix}=\begin{bmatrix} n_x & n_y & 0 & 0 & 0 \\ -n_y & n_x & 0 & 0 & 0 \\ 0 & 0 & 1 & 0 & 0 \\ 0 & 0 & 0 & n_x & n_y \\ 0 & 0 & 0 & -n_y & n_x \end{bmatrix}\begin{Bmatrix} u_0 \\ v_0 \\ w_0 \\ \varphi_x \\ \varphi_y \end{Bmatrix}=\boldsymbol{R}\boldsymbol{D}_0$$

$$\boldsymbol{R}=\begin{bmatrix} n_x & n_y & 0 & 0 & 0 \\ -n_y & n_x & 0 & 0 & 0 \\ 0 & 0 & 1 & 0 & 0 \\ 0 & 0 & 0 & n_x & -n_y \\ 0 & 0 & 0 & n_y & n_x \end{bmatrix}, \quad \boldsymbol{F}_{\boldsymbol{B}}=\begin{Bmatrix} \hat{N}_{nn} \\ \hat{N}_{ns} \\ \hat{Q}_n \\ \hat{M}_{nn} \\ \hat{M}_{ns} \end{Bmatrix} \tag{27}$$

Using four-noded elements, one may express the displacement vector based on the nodal values of the displacement parameters

$$\boldsymbol{D}_0^{(e)} = \begin{pmatrix} \psi_1 & 0 & 0 & 0 & 0 & \psi_4 & 0 & 0 & 0 & 0 \\ 0 & \psi_1 & 0 & 0 & 0 & 0 & \psi_4 & 0 & 0 & 0 \\ 0 & 0 & \psi_1 & 0 & 0 & \ldots. 0 & 0 & \psi_4 & 0 & 0 \\ 0 & 0 & 0 & \psi_1 & 0 & 0 & 0 & 0 & \psi_4 & 0 \\ 0 & 0 & 0 & 0 & \psi_1 & 0 & 0 & 0 & 0 & \psi_4 \end{pmatrix}_{5\times 20} \quad \boldsymbol{d}_0^{(e)} = \boldsymbol{\psi}\boldsymbol{d}_0^{(e)}$$
$$\boldsymbol{d}_0^{(e)T} = \left\langle u_{01} \quad v_{01} \quad w_{01} \quad \varphi_{x1} \quad \varphi_{y1} \quad \ldots\ldots \quad u_{04} \quad v_{04} \quad w_{04} \quad \varphi_{x4} \quad \varphi_{y4} \right\rangle^{(e)} \tag{28}$$

where $\boldsymbol{\psi}$ is the shape functions vector of the rectangular element [29]:

$$\psi_i = \tfrac{1}{4}\left(1+\xi_i\xi\right)\left(1+\eta_i\eta\right), \quad i = 1,2,3,4 \tag{29}$$

and ξ and η are the natural coordinates of the element, in the x and y directions, respectively. Therefore, the following vectors may be defined in relation to Eq. (26):

$$\boldsymbol{B}_1 = \boldsymbol{L}_1\boldsymbol{\psi}, \quad \boldsymbol{B}_2 = \boldsymbol{L}_2\boldsymbol{\psi}, \quad \boldsymbol{B}_3 = \boldsymbol{L}_3\boldsymbol{\psi}, \quad \boldsymbol{B}_4 = \boldsymbol{L}_4\boldsymbol{\psi} \tag{30}$$

Sine Eq. (26) has to be valid for any arbitrary time intervals, the integrand of the time integral should be set equal to zero:

$$\delta\left(\boldsymbol{d}_0^{(e)}\right)^t \left\{ \int_{\Omega_0^e} \left[\boldsymbol{B}_1^T(\boldsymbol{A}^e\boldsymbol{B}_2 + \boldsymbol{B}^e\boldsymbol{B}_3)\boldsymbol{d}_0^{(e)} + \boldsymbol{B}_3^T\left(\boldsymbol{B}^e\boldsymbol{B}_2 + \boldsymbol{D}^e\boldsymbol{B}_3\right)\boldsymbol{d}_0^{(e)} + k\boldsymbol{B}_4^T\boldsymbol{A}^*\boldsymbol{B}_4\boldsymbol{d}_0^{(e)} + \boldsymbol{\psi}^T\boldsymbol{I}\boldsymbol{\psi}\ddot{\boldsymbol{d}}_0^{(e)} \right.\right.$$
$$\left.\left. -\boldsymbol{\psi}^T\boldsymbol{q}^e \right] dxdy - \int_{\Gamma_\sigma^e} \boldsymbol{\psi}^T\boldsymbol{R}^T\boldsymbol{F}_{\boldsymbol{B}}^e dS - \boldsymbol{\psi}^T\boldsymbol{F}_{\boldsymbol{c}}^e \right\} = 0 \tag{31}$$

Eq. (31) holds for any arbitrary $\delta\left(\boldsymbol{d}_0^{(e)}\right)^t$. Thus, one may deduce that:

$$\int_{\Omega_0^e} \left[\boldsymbol{B}_1^T(\boldsymbol{A}^e\boldsymbol{B}_2 + \boldsymbol{B}^e\boldsymbol{B}_3)\boldsymbol{d}_0^{(e)} + \boldsymbol{B}_3^T\left(\boldsymbol{B}^e\boldsymbol{B}_2 + \boldsymbol{D}^e\boldsymbol{B}_3\right)\boldsymbol{d}_0^{(e)} + k\boldsymbol{B}_4^T\boldsymbol{A}^*\boldsymbol{B}_4\boldsymbol{d}_0^{(e)} + \boldsymbol{\psi}^T\boldsymbol{I}\boldsymbol{\psi}\ddot{\boldsymbol{d}}_0^{(e)} - \boldsymbol{\psi}^T\boldsymbol{q}^e \right] dxdy$$
$$- \int_{\Gamma_\sigma^e} \left[\boldsymbol{\psi}^T\boldsymbol{R}^T\boldsymbol{F}_{\boldsymbol{B}}^e \right] dS - \boldsymbol{\psi}^T\boldsymbol{F}_{\boldsymbol{c}}^e = 0 \tag{32}$$

or

$$\left(\boldsymbol{K}_{11} + \boldsymbol{K}_{22} + \boldsymbol{K}_{12}\right)^{(e)} \boldsymbol{d}_0^{(e)} + \boldsymbol{M}^e\ddot{\boldsymbol{d}}_0^{(e)} = \boldsymbol{F}^e \tag{33}$$

and in a compact form:

$$\boldsymbol{M}^e\ddot{\boldsymbol{d}}_0^{(e)} + \boldsymbol{K}^e\boldsymbol{d}_0^{(e)} = \boldsymbol{F}^e \tag{34}$$

where:

$$
\begin{aligned}
\boldsymbol{M}^e &= \int_{\Omega_0^e} \boldsymbol{\psi}^T \boldsymbol{I} \boldsymbol{\psi} dxdy \\
\boldsymbol{K}_{11}^e &= \int_{\Omega_0^e} \left[\boldsymbol{B}_1^T (\boldsymbol{A}^e \boldsymbol{B}_2 + \boldsymbol{B}^e \boldsymbol{B}_3) \right] dxdy \\
\boldsymbol{K}_{22}^e &= \int_{\Omega_0^e} \left[\boldsymbol{B}_3^T \left(\boldsymbol{B}^e \boldsymbol{B}_2 + \boldsymbol{D}^e \boldsymbol{B}_3 \right) \right] dxdy \\
\boldsymbol{K}_{12} &= \int_{\Omega_0^e} \left(k \boldsymbol{B}_4^T \boldsymbol{A}^* \boldsymbol{B}_4 \right) dxdy \\
\boldsymbol{F}^e &= \int_{\Omega_0^e} \left(\boldsymbol{\psi}^T \boldsymbol{q}^e \right) dxdy + \int_{\Gamma_\sigma^e} (\boldsymbol{\psi}^T \boldsymbol{R}^T \boldsymbol{F}_{\boldsymbol{B}}^e) dS + \boldsymbol{\psi}^T \boldsymbol{F}_{\boldsymbol{c}}^e
\end{aligned}
\tag{35}
$$

The system of Eq. (34) has to be solved with the indenter equation of motion

$$M_I \ddot{W}_I = -F_c \tag{36}$$

or

$$M_I \ddot{W}_I + k_c \left(W_I - d_I \right)^{3/2} = 0 \tag{37}$$

where M_I, W_I, and d_I are mass and displacement of the indenter, and lateral deflection of the impacted node of the plate, respectively. Based on the second-order Runge-Kutta numerical integration method [30], system of Eqs. (34) and (37) may be reduced to an algebraic system of equations.

$$
\begin{cases}
\bar{\boldsymbol{K}}_{n+1} \boldsymbol{d}_{n+1} = \bar{\boldsymbol{F}}_{n+1} \\
\left(W_I \right)_{n+1} = (W_I)_n + \Delta t (\dot{W}_I)_n + \dfrac{(\Delta t)^2}{4} (\ddot{W}_I)_n - \dfrac{(\Delta t)^2}{4 M_I} (F_c)_{n+1}
\end{cases}
\tag{38}
$$

where for example:

$$
\begin{aligned}
\left(F_c \right)_{n+1} &= k_c \left(\alpha_{n+1} \right)^{3/2} = k_c \left[\left(W_I \right)_{n+1} - \left(d_I \right)_{n+1} \right]^{3/2} \\
&= k_c \left[(W_I)_n + \Delta t (\dot{W}_I)_n + \frac{(\Delta t)^2}{4} (\ddot{W}_I)_n - \frac{(\Delta t)^2}{4 M_I} \left(F_c \right)_{n+1} - (d_I)_{n+1} \right]^{3/2}
\end{aligned}
\tag{39}
$$

and

$$
\begin{aligned}
\bar{\boldsymbol{K}}_{n+1} &= \boldsymbol{K}_{n+1} + \frac{1}{\beta (\Delta t)^2} \boldsymbol{M} \\
\bar{\boldsymbol{F}}_{n+1} &= \boldsymbol{F}_{\boldsymbol{B} n+1} + \left(\boldsymbol{F}_{\boldsymbol{c}} \right)_{n+1} + \boldsymbol{M} \left(\frac{1}{\beta (\Delta t)^2} \boldsymbol{d}_n + \frac{1}{\beta \Delta t} \dot{\boldsymbol{d}}_n + \frac{1 - 2\beta}{2\beta} \ddot{\boldsymbol{d}}_n \right) \\
\left(\boldsymbol{F}_{\boldsymbol{c}} \right)_{n+1} &= \left(F_c \right)_{n+1} \{ \boldsymbol{I} \}, \qquad I_i = \begin{cases} 0 & , i \neq 5 * \text{center node number} - 2 \\ 1 & , i = 5 * \text{center node number} - 2 \end{cases}
\end{aligned}
\tag{40}
$$

and n is the time step counter. Since the resulting system of equations is highly nonlinear, solutions associated with each time step may be determined based on an iterative procedure.

For a simply supported plate, the following boundary and initial conditions may be chosen:

$$\text{at } x=0,a: \ \ w,\ \varphi_y=0$$
$$\text{at } y=0,b: \ \ w,\ \varphi_x=0 \tag{41}$$

$$\boldsymbol{d}_0,\dot{\boldsymbol{d}}_0=\boldsymbol{0}\ ,\alpha_0=0,\dot{\alpha}_0=V_0 \tag{42}$$

The initial acceleration may be determined as

$$\ddot{\boldsymbol{d}}_0=\boldsymbol{M}^{-1}\left(\boldsymbol{F}_0-\boldsymbol{K}\,\boldsymbol{d}_0\right) \tag{43}$$

However, since Eq. (38) is a nonlinear equation, a Picard or Newton-Raphson technique has to be used in each time step to reach a convergent solution. The following convergence criterion is employed in the present paper

$$\frac{\left\|\boldsymbol{d}_n^{(m+1)}-\boldsymbol{d}_n^{(m)}\right\|}{\left\|\boldsymbol{d}_n^{(m+1)}\right\|}\cong\in \tag{44}$$

where m is the iteration counter and $\in$ is a sufficiently small number. In the present research, $\in=0.0001$ is used as a convergence criterion.

4 RESULTS AND DISCUSSIONS

In the present section, after validation of the results, influence of the in-plane in-phase/anti-phase biaxial preloads and eccentricity of the impact are studied, in addition to the other parametric studies. Since the numerical time integration procedures manifest an error accumulation phenomenon that is especially affected by the time integration steps and in order to trace the time history of the quantities more adequately, the integration time steps have to be much less than the fundamental period time of the structure and especially much less than the response time of the structure. For this reason, a time step that is equal or less than 10^{-6} (sec) is adopted.

Some characteristics of the impact are investigated in the present section for the first time. For derivation of the results, the plate is discretized into rectangular elements, as shown in Fig. 1.

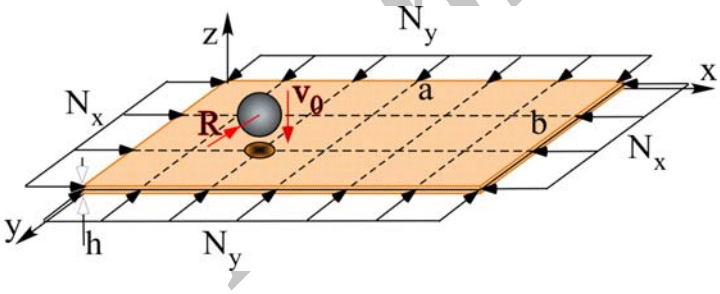

Fig.1
Geometric parameters and the coordinates system of the considered preloaded functionally graded composite plate under the low-velocity impact.

4.1 Verification of the results

To verify results of the present formulations and results, an example previously adopted by Tiberkak et. al. [31] is chosen. The plate is simply supported and has $0.127*0.0762*0.00465\text{m}^3$ dimensions. Material properties and geometric data of the fiber reinforced composite $[45/90/-45/0]_{3S}$ plate and indenter are as follows [31]:

$$\text{Plate: } E_1=129GPa,\ E_2=7.5GPa,\ G_{12}=3.5GPa,\ \nu_{12}=0.33,\ \rho=1540kgm^{-3}$$
$$\text{Impactor : } R=12.7mm,\ E=207GPa,\ \nu=0.3$$

Mass and initial velocity of the indenter are *0.314 kg* and *2.92 m/s*, respectively. Present results for the contact force are compared with results of Tiberkak et al. [31] in Fig. 2. Tiberkak et al. used a finite element formulation based on

the first-order shear deformation plate theory, but considered the central impact and determined in determination of the stiffness of the contact region, ignored influence of the stiffness of the underneath layers on the apparent contact stiffness of the plate. However, as Fig. 2 reveals, there is a good agreement between present results and results of Tiberkak et al.

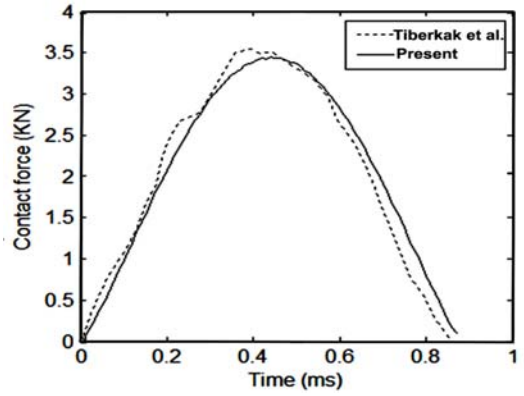

Fig.2
Time histories of the contact force predicted by present formulation and Tiberkak et al. [31].

4.2 Influence of various parameters on characteristics of the low-velocity impact characteristics of responses of *the plate.*

For in the present and next sections, the following information is employed for the steel indenter and the asymmetric [0/90/0/90/0/90/0/90/0/90] graphite/epoxy laminated composite plate, unless otherwise stated [32]:

$$E_1 = 120GPa,\ E_2 = 7.9GPa,\ G_{12} = G_{13} = G_{23} = 5.5GPa,\ \nu_{12} = 0.33,\ \rho = 1580kgm^{-3}$$
$$h = 4.538mm,\ R = 6.6mm,\ M = 8.54g,\ E = 207GPa,\ \nu = 0.3$$

Dimensions of the plate are 20x20x0.269 cm. It is assumed that the plate is impacted through a central/eccentric low-velocity impact by a steel indenter with a spherical nose. The boundary conditions. All edges of the plate are clamped and immovable .

The original responses and influence of the indenter velocity on the indentation, contact force, and lateral deflection of the plate are illustrated in Figs. 3 to 5, respectively. As it may be expected, magnitudes of all responses are have increased with an increase in the indenter velocity. Although the maximum contact force has occurred in a time instant that is almost coincident with that of the maximum indentation value (this is evident only if a static contact with a half space occurs), the maximum lateral deflection of the plate has occurred in a quite different time instant. Influence of the higher vibration modes of the plate on time histories of the responses may be easily detected in Figs. 3 to 5.

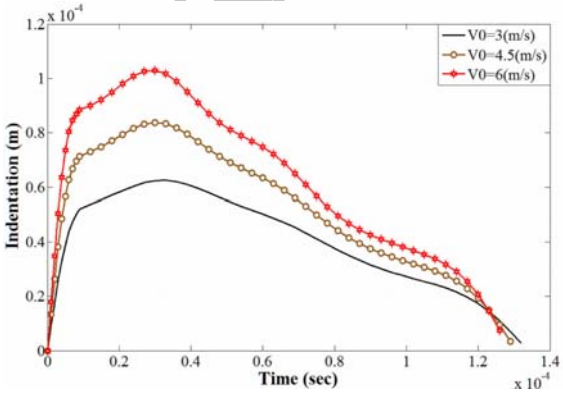

Fig.3
Effect of the initial velocity of the indenter on time history of the indentation.

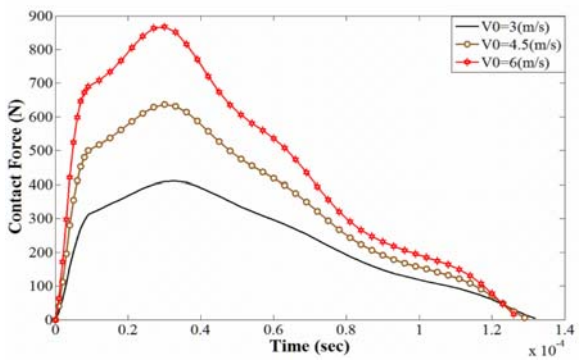

Fig.4
Effect of the initial velocity of the indenter on time history of the contact force.

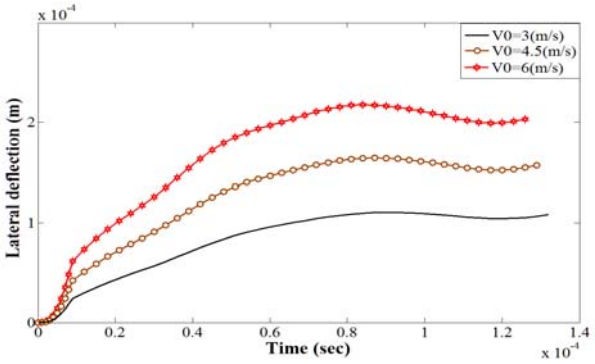

Fig.5
Effect of the initial velocity of the indenter on time history of the lateral deflection of the plate.

Influence of the radius (and simultaneously, mass) of the indenter are investigated through studying the time histories of the indentation, contact force, and lateral deflection plotted in Figs. 6 to 8. In this regard, the following cases are considered:

$R_1 = 6.6mm,\ M_1 = 8.54\ kg,\ k_c = 8.3e8$
$R_2 = 7.3mm,\ M_2 = 1.5M_1,\ k_c = 8.7e8$
$R = 8.1mm,\ M = 2M_1,\ k_c = 9e8$

Other parameters are similar to the base values. As it may be seen from Figs. 6 to 8, amplitudes of the indentation, contact force and lateral deflection increase with an increase in the indenter radius/mass. Furthermore, the contact duration time increases with the indenter mass. Influence of the plate thickness may be deduced from Figs. 9 to 11. Increased thickness of the plate leads to increased bending stiffness for the plate. Therefore, the lateral movability (lateral deflection) of the plate decreases and consequently, the indentation and contact force of the plate increase.

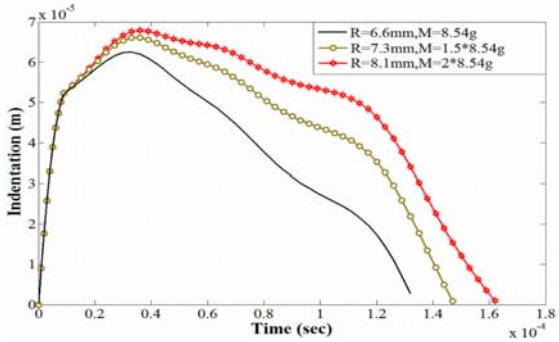

Fig.6
Effect of the mass and radius of the indenter on time history of the indentation.

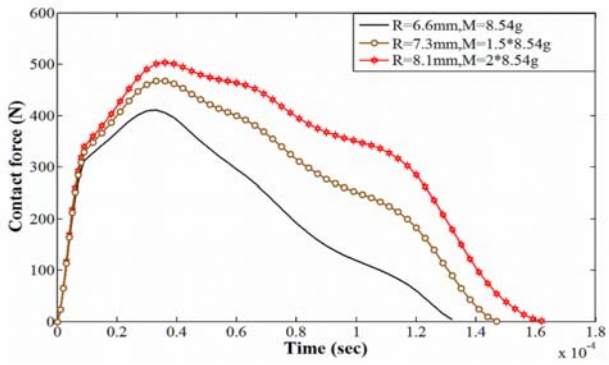

Fig.7
Effect of the mass and radius of the indenter on time history of the contact force.

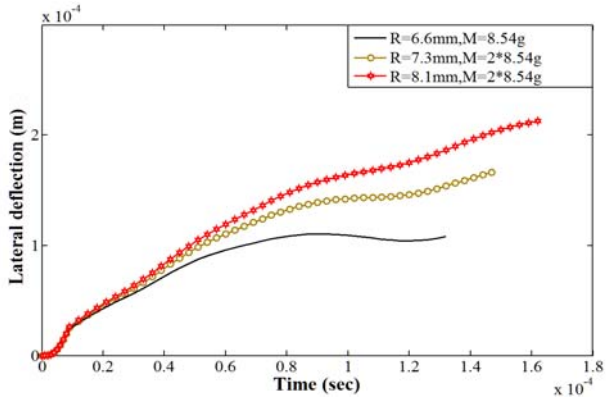

Fig.8
Effect of the mass and radius of the indenter on time history of the lateral deflection of the plate.

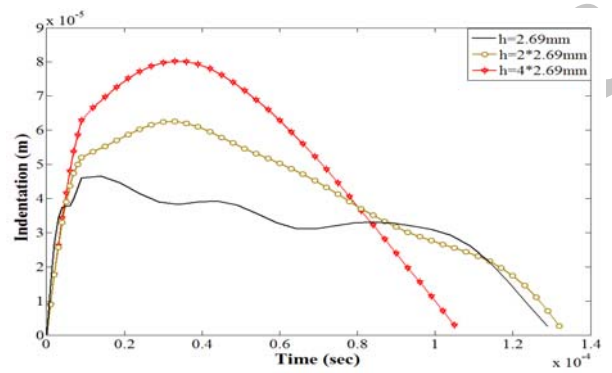

Fig.9
Effect of the plate thickness on time history of the indentation.

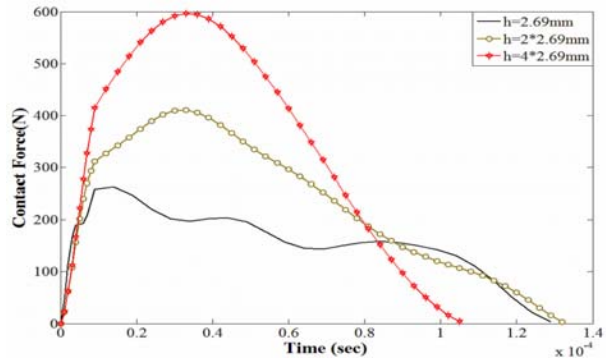

Fig.10
Effect of the plate thickness on time history of the contact force.

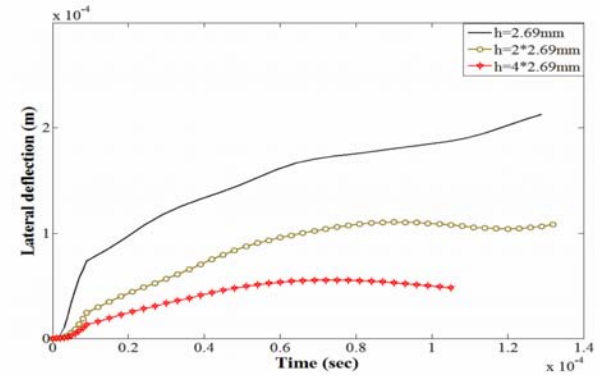

Fig.11
Effect of the plate thickness on time history of the lateral deflection of the plate.

4.3 Effects of the eccentric impact

To investigate effects of an eccentric low-velocity impact on the considered laminated composite plate, the impacted point is chosen among the eccentric nodal points. Location of the mentioned nodal point is shown in Fig. 12. Time history of the contact force is plotted in Fig. 13 for both central and eccentric impacts. The apparent stiffness (hardness) of the contact region show no remarkable change. Although the overall bending stiffness of the contact region has been increased (due to less movability in the neighborhood of the clamped edges), due to the increases occurred in the distances relative to some corners of the plate, the overall bending stiffness of the plate has decreased and consequently, the contact time duration has increased.
Time histories of the lateral deflection of the plate are compared in Fig. 14 , for the central and eccentric impacts.

For eccentric impact, time histories of lateral deflections of both the impacted point and the center point of the plate are plotted. As it may readily be noticed, there is a delay between response of the impacted point and that of the center point of the eccentric impact. The lag time is required to enable the traveling waves following the impact to reach the center point of the plate. Moreover, the lag between the maximum indentation time and the time instant of maximum lateral deflection is smaller for the eccentric impact case.

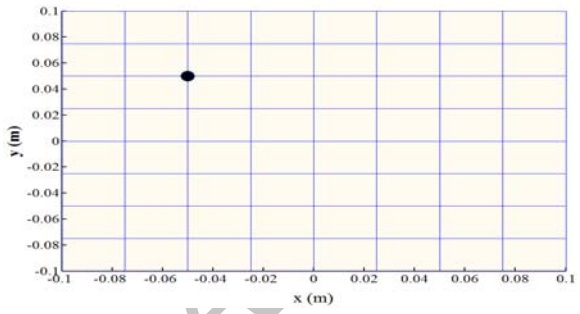

Fig.12
Dimensions of the plate and location of the eccentric impact.

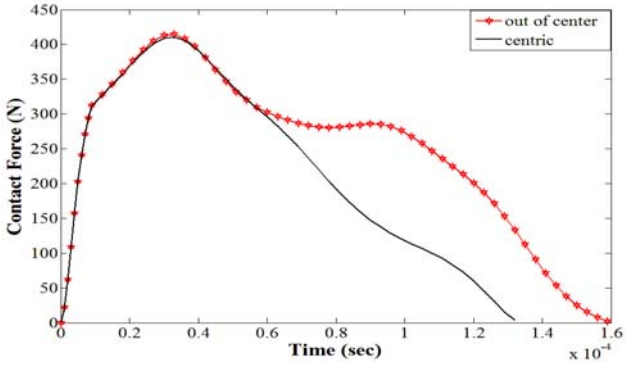

Fig.13
Time histories of the contact force for the central and eccentric impacts.

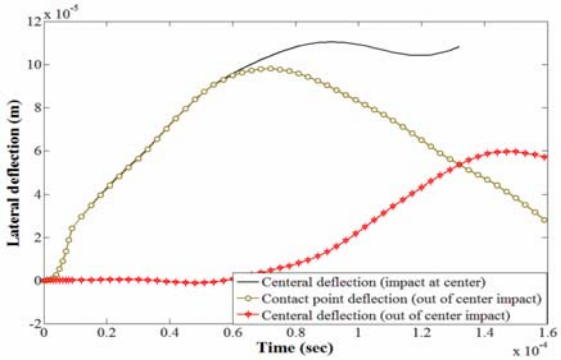

Fig.14
A comparison between time histories of the lateral deflection of the plate for central and eccentric impacts.

4.4 Effect of the in-plane preloads

To evaluate effects of the initial stresses on the impact responses of the laminated composite plate, a plate with material properties and geometric parameters similar to those mentioned in the preceding sections is considered. Effect of imposing biaxial in-plane tensile preload on time histories of the indentation, contact force, and lateral deflection of the plate are illustrated in Figs. 15 to 17, respectively. In this regard, in-plane tension preloads with magnitudes 0, 10, 40, 60, and 100 kN are considered. Therefore, effects of high preloads are investigated. Results presented in Figs. 15 to 17 confirm that the tensile preloads increase both the contact force and indentation and generally, decrease the lateral deflection of the plate.

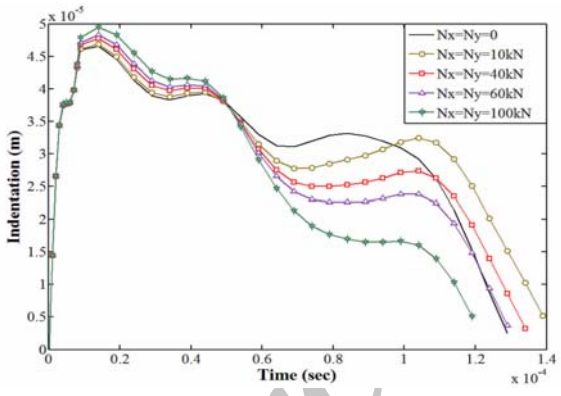

Fig.15
Effects of the tensile preloads on the indentation time history of the laminated composite plate.

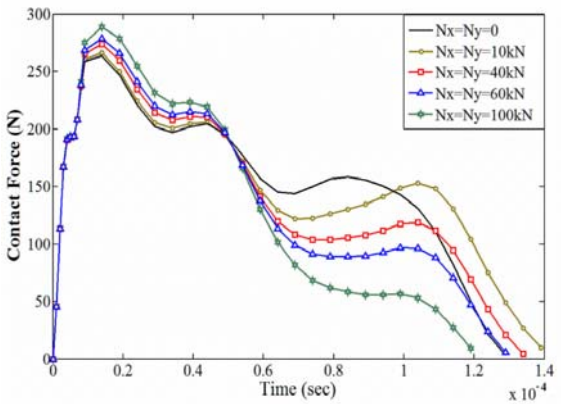

Fig.16
Effects of the tensile preloads on the contact force time history of the laminated composite plate.

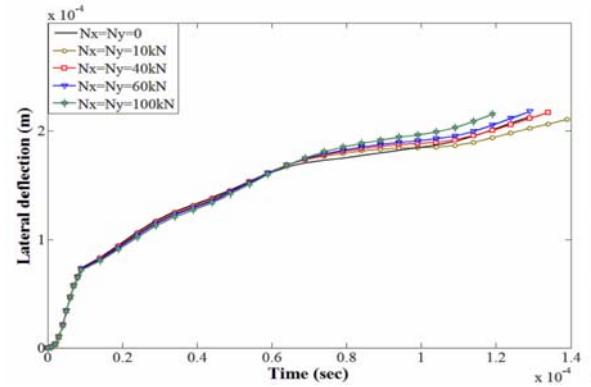

Fig.17
Effects of the tensile preloads on the lateral deflection of the laminated composite plate.

Effect of the biaxial tensile and compressive loads as well as tensile-compressive preloads on the contact force and lateral deflection of the plate are compared in Figs. 18 and 19. Since the compressive loads generally tend to create larger lateral deflections than in comparison with the tensile loads (and in the limit, lead to buckling), the lateral deflection has a greater contribution in absorption of the impact energy in case of a compressive preload. Therefore, the plate will have a greater movability and consequently, experience less indentations and contact force. Fig. 18 confirms this issue since the resulting contact force (and subsequently, the indentation) is greater for the tensile preloads. However, the anti-phase case (i.e., associated with the tensile-compressive preloads), has led to results similar to those of the compressive preloads; an evident that reveal the dominant effect of the compressive preloads.

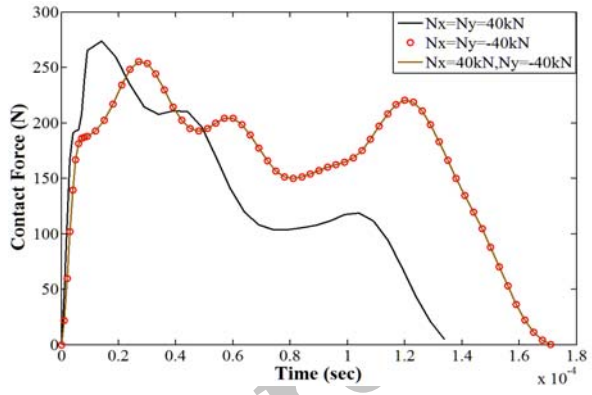

Fig.18
A comparison between time histories of the contact force predicted by corresponding to the in-phase and anti-phase preloads.

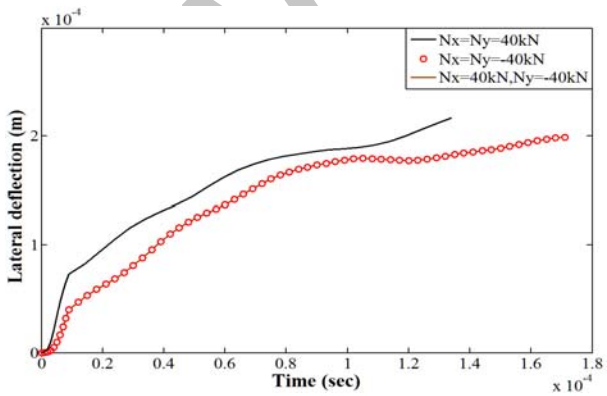

Fig.19
A comparison between time histories of the contact force predicted by corresponding to the in-phase and anti-phase preloads.

5 CONCLUSIONS

In the present paper, a nonlinear eccentric low-velocity impact analysis is presented for laminated composite plates subjected to eccentric impacts and biaxial in-plane in-phase or anti-phase preloads.

Some of the novelties included in the present research are:

- Considering the more general case of an eccentric impact, for the first time.
- Evaluating effects of various types (i.e., in-phase and anti-phase) preloads, especially, on the indentation and contact force.
- Using nonlinear strain-displacement expressions.
- Presenting a complete formulation and a solution technique instead of using commercial softwares.

Among other conclusions, results reveal that compressive and anti-phase tensile-compressive loads preloads lead to greater contact forces and indentations and consequently, higher damages.

REFERENCES

[1] Gong S.W., Lam K.Y., 2000, Effects of structural damping and stiffness on impact response of layered structures, *Amerian Institute of Aeronautics and Astronautics* **38**(9): 1730–1735.

[2] Jacquelin E., Laine´ J.-P., Bennani A., Massenzio M., 2007, A modelling of an impacted structure based on constraint modes, *Journal of Sound and Vibration* **301**(3-5), 789–802 .

[3] Pashah S., Massenzio M., Jacquelin E., 2008, Prediction of structural response for low velocity impact, *International Journal of Impact Engineering* **35**(2): 119–132 .

[4] Anderson T.A., 2005, An investigation of SDOF models for large mass impact on sandwich composites. *Journal Composites: Part B* **36**(2): 135–142.

[5] Abrate S., 1997, Localized impact on sandwich structures with laminated facing, *Applied Mechanics Reviews* **50**(2): 69–82.

[6] Abrate S., 2011, *Impact Engineering of Composite Structures*, CISM, Udine, Springer.

[7] Chai G.B., Zhu S., 2011, A review of low-velocity impact on sandwich structures, *Proceedings of the Institution of Mechanical Engineers, Part L: Journal of Materials-Design and Applications* **225**(4): 207-230 .

[8] Qiu X.M., Yu T.X., 2011, Some topics in recent advances and applications of structural impact dynamics, *Applied Mechanics Reviews* **64**(3).

[9] Nosier A., Kapania R.K., Reddy J.N., 1994, Low-velocity impact of laminated composites using a layerwise theory, *Computational Mechanics* **13**: 360- 379.

[10] Sun D., Luo S.-N., 2011, Wave propagation and transient response of a FGM plate under a point impact load based on higher-order shear deformation theory, *Composite Structures* **93**: 1474–1484.

[11] Yigit A.S., Christoforou A.P., 1995, On the impact between a rigid sphere and a thin composite laminate supported by a rigid substrate, *Composite Structures* **30**(2):169–177.

[12] Christoforou A.P., Yigit A.S., 1998, Effect of flexibility on low velocity impact response, *Journal of Sound and Vibration* **217:** 563–578 .

[13] Yigit A.S., Christoforou A.P., 2007, Limits of asymptotic solutions in low-velocity impact of composite plates, *Composite Structures* **81**: 568–574.

[14] Christoforou A.P., Yigit A.S., 2009, Scaling of low-velocity impact response in composite structures, *Composite Structures* **91**: 358–365.

[15] Shariyat M., Ghajar R., Alipour M.M., 2012, An analytical solution for a low velocity impact between a rigid sphere and a transversely isotropic strain-hardening plate supported by a rigid substrate, *Journal of Engineering Mathematics* **75**: 107-125.

[16] Guan Z., Yang C., 2002, Low-velocity impact and damage process of composite laminates, *Journal Composites Material* **36**, 851-871.

[17] Zheng D., Binienda W.K., 2009, Semianalytical solution of wave-controlled impact on composite laminates, *ASCE Journal of Aerospace Engineering* **22**: 318-323.

[18] Olsson R., 2010, Analytical model for delamination growth during small mass impact on plates, *International Journal of Solids and Structures* **47:** 2884–2892.

[19] Yang J., Shen H.-S., 2001, Dynamic response of initially stressed functionally graded thin plates, *Composite Structures* **21**: 497-508.

[20] Choi I.-H., 2008, Low-velocity impact analysis of composite laminates under initial in-plane load, *Composite Structures* **86**, 251–257.

[21] Shariyat M., Farzan F., 2012, Nonlinear eccentric low-velocity impact analysis of a highly pre-stressed FGM rectangular plate, using a refined contact law, *Archive of Applied Mechanics*, DOI: 10.1007/s00419-012-0708-3.

[22] Shariyat M., Jafari R., 2013, Nonlinear low-velocity impact response analysis of a radially preloaded two-directional-functionally graded circular plate: A refined contact stiffness approach, *Composites Part B* **45**: 981-994.
[23] Khalili S.M.R., Mittal R.K., Mohammad Panah N., 2007, Analysis of fiber reinforced composite plates subjected to transverse impact in the presence of initial stresses, *Composite Structures* **77**: 263–268.
[24] Heimbs S., Heller S., Middendorf P., Ha¨hnel F., Weiße J., 2009, Low velocity impact on CFRP plates with compressive preload: Test and modeling, *International Journal of Impact Engineering* **36**: 1182–1193.
[25] Choi I.H., 2008, Low-velocity impact analysis of composite laminates under initial in-plane load, *Composite Structures* **86**: 251–257.
[26] Reddy J.N., 2006, *Theory and Analysis of Elastic Plates and Shells*, 2nd edition, CRC Press.
[27] Turner J.R., 1980, Contact on a transversely isotropic half-space, or between two transversely isotropic bodies, *International Journal of Solids and Structures* **16**: 409–19 .
[28] Yang S.H., Sun C.T., 1982, Indentation law for composite laminates, in: Composite Materials *, Testing and Design (6th conference)*, ASTM STP-787, 425–449.
[29] Huebner K.H., Dewhirst D.L., Smith D.E., Byrom T.G., 2001, *The Finite Element Method for Engineers*, 4th Edition, John Wiley & Sons.
[30] Bathe K.-J., 2007, *Finite Element Procedures*, Cambridge.
[31] Tiberkak R., 2008, Damage prediction in composite plates subjected to low velocity impact, *Composite Structures* **83**: 73–82.
[32] Pierson M.O., Vaziri R., 1996, Analytical solution for low-velocity impact response of composite plates, *Amerian Institute of Aeronautics and Astronautics* **34**: 1633-1640.